

Article

Study on the Optimized Muffler with Function of PM Filtration for Non-Road Diesel Engines

Long Feng ¹, Lizhuang Dou ¹, Xiang Wen ¹, Mingfei Mu ^{1,2,*}, Xiaotong Ma ¹, Bisheng Chen ¹, Chao Shi ^{2,3,*} and Xiude Hu ⁴

¹ College of Mechanical and Electronic Engineering, Shandong University of Science and Technology, Qingdao 266590, China; longfeng@sdust.edu.cn (L.F.); doulizhuang@sdust.edu.cn (L.D.); hnwenxiang@sdust.edu.cn (X.W.); xiaotongma@sdust.edu.cn (X.M.); bishegch@sdust.edu.cn (B.C.)

² School of Transportation Science and Engineering, Beihang University, Beijing 100083, China

³ Beijing DiDi Infinity Technology and Development Co., Ltd., Beijing 100193, China

⁴ State Key Laboratory of High-Efficiency Utilization of Coal and Green Chemical Engineering, Ningxia University, Yinchuan 750021, China; xiudehu@nxu.edu.cn

* Correspondence: mingfei@sdust.edu.cn (M.M.); chaoshichao@didiglobal.com (C.S.)

Abstract: With a high thermal efficiency, high reliability and good fuel economy, diesel engines have been widely used. However, with the increasingly stringent standards regarding non-road diesel engine emissions, diesel engines can hardly satisfy the particle emission requirements through internal purification alone. To reduce the particle emission and noise levels of the non-road diesel engine R180, this paper optimized the original muffler, and endowed the muffler with a particulate matter (PM) filtering function to improve the muffling. This study first proposed stainless steel fiber as the filtering medium as it is inexpensive and accessible; a bench experiment was conducted to verify the particle filtration performance and its effect on the overall engine performance. Then, the structure of the existing muffler in non-road diesel engines R180 was optimized, and the stainless steel fiber filtering was integrated. The internal flow field of the optimized muffler was obtained in the computational fluid dynamics software FLUENT, and the acoustic and filtration performance was studied. The experimental and simulation results indicated that the optimized muffler could achieve both particle filtration and noise reduction.

Keywords: non-road diesel engine; stainless steel fiber; particle filtration; noise reduction



Citation: Feng, L.; Dou, L.; Wen, X.; Mu, M.; Ma, X.; Chen, B.; Shi, C.; Hu, X. Study on the Optimized Muffler with Function of PM Filtration for Non-Road Diesel Engines. *Atmosphere* **2022**, *13*, 350. <https://doi.org/10.3390/atmos13020350>

Academic Editor: Yongming Han

Received: 10 January 2022

Accepted: 12 February 2022

Published: 19 February 2022

Publisher's Note: MDPI stays neutral with regard to jurisdictional claims in published maps and institutional affiliations.



Copyright: © 2022 by the authors. Licensee MDPI, Basel, Switzerland. This article is an open access article distributed under the terms and conditions of the Creative Commons Attribution (CC BY) license (<https://creativecommons.org/licenses/by/4.0/>).

1. Introduction

With the rapid development of the economy in China over the last 40 years, environmental problems caused by the massive consumption of energy have occurred [1,2]. Among these issues, the problem of atmospheric compound pollution characterized by particulate matter (PM) has attracted much attention from the government and public [3–5]. To alleviate air pollution problems, the government has adopted a series of air pollution prevention and control policies [6], including formulating ultralow emission standards for coal-fired power plants, reducing outdated production capacity, strengthening industrial emission standards, phasing out small-scale high-emission factories, installing volatile organic compound (VOC) emission control facilities, eliminating small coal-fired industrial boilers, applying electricity and natural gas to replace domestic coal burning, raising motor vehicle emission standards, and discontinuing old motor vehicles. With the continuous implementation of these measures, the air pollutants emitted by power plants, industrial sources, and road mobile sources have plummeted. However, the emissions of non-road mobile machinery have increasingly become prominent.

The “Technical Guidelines for the Compilation of Non-road Mobile Source Emission Inventories” defined non-road mobile machinery as mainly construction and agricultural

machinery [7]. In recent years, with the continuous acceleration of the agricultural mechanization process in China, the total diesel power of agricultural machinery increased from 867 million kW in 2014 to 797 million kW in 2019. The China Mobile Source Environmental Management Annual Report (2021) demonstrated that non-road mobile sources had similar PM and NO_x emissions to motor vehicles [8]. The impact of emissions originating from non-road mobile sources on the air quality cannot be ignored. Non-road mobile sources emit 163,000 tons of sulfur dioxide (SO₂), 425,000 tons of hydrocarbons (HCs), 4,782,000 tons of NO_x, and 237,000 tons of PM. The NO_x and PM emissions of non-road mobile machinery account for approximately 70% of the emissions of non-road mobile sources; among these emissions, the PM emissions of agricultural machinery account for 34.9% of the total emissions of non-road mobile sources, which verifies that agricultural machinery has become one of the main pollution sources of PM and NO_x.

Therefore, non-road mobile machinery emission characteristic analysis, pollutant concentration contribution analysis, etc., are urgently needed to provide scientific advice for the next step in the formulation of non-road machinery emission control measures.

At present, scholars have performed research work on the emissions of non-road mobile machinery. Lang et al. applied emission factor methods based on the fuel consumption to estimate the emissions of agricultural machinery in China [9]. Desouza et al. studied non-road mobile machinery emissions in London [10]. Guo et al. calculated pollutant emissions originating from agricultural and construction machinery in Beijing–Tianjin–Hebei based on the fuel consumption [11]. Zheng et al. established emissions stemming from construction machinery in Tianjin [12]. Hou et al. determined emissions of typical agricultural machinery in Beijing [13], and scholars have compiled emission inventories for non-road mobile machinery in Guangdong Province with the emission factor method based on the production power [14,15]. Li and Wang et al., established 2012 and 2013 Chinese non-road mobile source emission inventories, respectively, covering emissions of non-road mobile machinery [16,17], while non-road mobile source emission inventories for Chengdu, Mianyang, Northeast China, and Tianjin, including emissions originating from non-road mobile machinery, were also established [18–20]. Due to the limitation of data acquisition, many of the abovementioned studies relied on a relatively approximate fuel consumption-based method to estimate the emissions of non-road mobile machinery while ignoring differences in the holdings, working hours and production power levels between different types of machinery.

In addition, a series of non-road mobile source emission calculation models has been developed. These models can be employed to calculate the pollutant emissions of different non-road mobile machinery, such as the Non-road Engine Emissions Model (NONROAD) recommended by the U.S. Environmental Protection Agency [21], the California Air Resources Board recommended OFFROAD model [22], and the European Monitoring and Evaluation Programme (EMEP)/Core Inventory of Air Emissions (CORINAIR) model recommended by the European Environmental Protection Agency [23]. Lewis et al. estimated the HC, CO, PM, and NO_x emissions of non-road vehicles based on existing data of the NONROAD model published by the U.S. Environmental Protection Agency and data collected with an on-board emission test system [24].

To control the pollutant emission of non-road mobile machinery and further improve the air quality, the United States, European Union and Japan have all formulated non-road machinery emission regulations. In 1998, the United States formally promulgated first-phase (Tier 1) emission standards for non-road machinery, which clearly stipulated the emission limits of CO, HC, NO_x and PM. Subsequently, more stringent regulations were issued from 2000–2008, i.e., second-stage (Tier 2) and third-stage (Tier 3) emission standards. After 2008, fourth-stage (Tier 4) emission standards were promulgated to further reduce the emission limits of NO_x and PM and sulfur content in diesel [25,26]. The EU's first non-road machinery emission regulation was passed in the form of legislation in 1998. This regulation was divided into two stages according to non-road machinery engines. Subsequently, the EU formulated third- and fourth-phase emission standards and stipulated

that the third phase should be implemented from 2006–2013 and the fourth phase should be implemented after 2014 [27,28]. Japan implemented non-road machinery emission regulations in 2006 and subsequently introduced corresponding emission limits four times from 2006–2008 based on the output power [29]. In 2007, China issued the “Emission Limits and Measurement Methods for Diesel Engine Exhaust Pollutants for Non-road Mobile Machinery (China Phase I and Phase II)” and implemented this standard in the same year [30]. The first phase of emission standards stipulated different ratings of the CO, HC, NO_x and PM emission limits under power, while the second phase supplemented PM emission limits within the range from 0–18 kW. Subsequently, the Emission Limits and Measurement Methods for Exhaust Pollutants of Non-road Mobile Machinery with Diesel Engines (China Phase III and IV) was released and implemented in 2014 [31]. These third- and fourth-phase emission standards enhanced the control requirements for non-road mobile machinery above 560 kW. The Emission Control Technical Requirements for Non-road Diesel Mobile Machinery was released in 2020 and is a supplement to the China Phase IV standards, further tightening the emission limits of various pollutants [8,32]. The standards at each stage clearly stipulated the CO, HC, NO_x and PM emission limits for non-road mobile machinery under different power distributions. In September 2018, China promulgated and implemented the Limits and Measurement Methods for Exhaust Smoke from Non-road Mobile Machinery Equipped with a Diesel Engine [33], which provided a legal basis for regulatory authorities to strengthen the supervision of non-road mobile machinery emissions.

To satisfy the fourth-stage emission limit requirements, non-road machinery emission control technology can be divided into two categories: reduction in the original engine emissions and aftertreatment technology [34,35]. Reducing the original engine emissions refers to the reduction in NO_x and PM emissions through diesel optimization design, advanced fuel injection, exhaust gas recirculation (EGR), and the use of high-quality fuel oil and other in-engine exhaust purification technologies [36]. Currently, the commonly adopted non-road mechanical diesel engine exhaust gas aftertreatment technologies include diesel oxidation catalyst (DOC), diesel particulate filter (DPF), selective catalytic reduction (SCR) and other aftertreatment control technologies to reduce PM and NO_x in exhaust gas at the fourth stage [32,37].

With the continuous tightening of non-road machinery emission regulations, it is difficult to achieve the above emission standards by employing a certain aftertreatment technology alone. Therefore, a reasonable combination of aftertreatment technologies is the current mainstream approach. DOC+DPF imposes a significant effect on NO_x and PM reduction [38]. Zhang et al. installed DOC and particle oxidation catalytic converter (POC) devices in non-road diesel engines to satisfy China IV emission standards, and the PM value was greatly reduced, as determined in experimental research [39]. Guan et al. compared smoke and gaseous pollutant (NO_x, HC, and CO) data before and after the installation of DOC+POC technology and found that the PM and smoke emissions of non-road diesel engines after DOC+POC device installation could be reduced by 34~69% and 37~68%, respectively, and DOC+POC aftertreatment device installation fully satisfied the fourth-stage emission standards for non-road machinery within the 19~56 kW power range [40].

At present, most particulate filters installed in the non-road machinery are transplanted from traditional automotive particulate filters, and the material and installation costs are relatively high for non-road machinery, especially the agricultural machinery. Traditional automotive DPF exhibit a large filtering area and great pressure drop, which are unsuitable for non-road machinery with a low horsepower level. Currently, particulate filters that are especially designed for non-road machinery are really rare.

Aiming at the emission problem of non-road machinery, an optimized muffler with particle filtration was specifically designed for the single-cylinder diesel engine R180 of non-road machinery. Stainless steel fibers were employed as the filtration medium due to their low cost and easy access, which are suitable for small diesel engine, and the performance

was experimentally verified. Moreover, noise reduction design was conducted. Finally, the filtrating and muffling function of the optimized muffler were verified through experiments and simulations.

2. Materials and Methods

In this section, an experimental bench of the R180 diesel engine is established, the exhaust temperature, fuel consumption rate, and HC, CO, NO_x and CO₂ volume fractions in the exhaust under different working conditions are measured to verify the influence of the stainless steel fiber PM filter on the working performance, and the extinction coefficient of the exhaust is measured to verify the filtration performance. Then, based on the filtration effect of stainless steel fibers on PM emissions, the original muffler in the R180 diesel engine is structurally improved, and an integrated PM filtration and noise elimination device is designed that can be quickly disassembled, which increases the device compactness while enhancing the noise reduction and filtration effects.

2.1. Setup for the Validation of the Filtration Performance of Stainless Steel Fiber

Schematic diagrams of the test bench are shown in Figures 1 and 2. The bench comprises a dynamometer, diesel engine, particulate filter, electronic balance, temperature measuring instrument, gas analyzer and smoke meter. The diesel engine (Changchai R180, Changchai Co., Ltd., Changzhou, China shown in Table 1) is connected to the dynamometer. The dynamometer (CW50, CAMA Electromechanic Co., Ltd., Luoyang, China) is employed to measure the speed and torque of the diesel engine under different operating conditions. The electronic balance (LT500B, Tianliang Instrument Co., Ltd., Changshu, China) is employed to measure the fuel consumption. The gas analyzer (FGA-4100, Foshan Analytical Instrument Co., Ltd., Foshan, China) measures the HC, CO, NO, and CO₂ volume percentages in the exhaust gas. The temperature measuring instrument applies a K-type thermocouple to measure the exhaust temperature, and a stainless steel fiber particle filter is implemented to collect PM. The smoke meter (AVL DiSmoke 4000, AVL List GmbH, Graz, Austria) is employed to detect the PM content. Table 2 lists the eight settings of the diesel engine at different speeds in the experiment.



Figure 1. Experimental bench of R180.

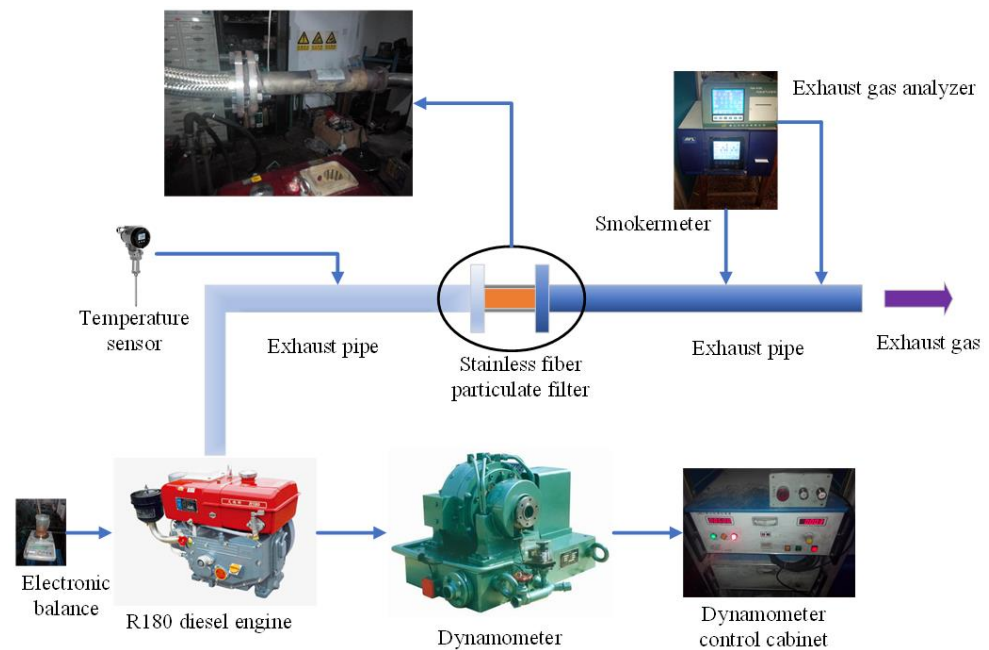


Figure 2. Schematic diagram of the bench.

Table 1. Parameters of the R180 diesel engine.

Name	Value
Cylinder diameter/mm	80
Stroke/mm	80
Cooling type	Evaporative water
Compression ratio	21
Rated horsepower/kW	5.67 (2600 r/min)
Specific fuel consumption/g/kW·h	≤278.8
Specific oil consumption/(g/(kW·h))	≤3.4
Injection pressure/MPa	13.72 ± 0.5
Lubricating type	Splash lubrication
Dry weight/kg	72
Overall dimension/mm	625 × 341 × 466

Table 2. Experimental parameters.

Load, %	Installation Setting of the Stainless Fiber Particulate Filter	Label
25	*	a
25	&	A
50	*	b
50	&	B
75	*	c
75	&	C
100	*	d
100	&	D

Note: “*” indicates that a particulate filter is installed; “&” indicates that a particulate filter is not installed.

In the experiment, stainless steel fibers were applied as the filter medium, and the cross section of the selected stainless steel fibers was 0.45 mm × 3.56 mm. The volume was 30 mL, as measured by a syringe with a diameter of 36 mm under a pressure of 0.5 MPa, the weight was 19.5 g, the density of the stainless steel fiber reached 7.8 g/cm³, and the porosity was calculated as 91.7%. To ensure the filtration efficiency, in the stainless steel fiber particulate filter, four stainless steel fiber balls were connected in series with iron wires, the series-connected stainless steel fiber balls were contained in a thin-walled aluminum

tube, and the stainless steel fiber balls were tightened with iron wires. The stainless steel fiber balls were compressed to the minimum porosity under the tightening force of the iron wires, and the minimum porosity could be maintained to ensure the filtration efficiency. Moreover, the setup could be modularized to facilitate rapid disassembly of the stainless steel fiber particulate filter, as shown in Figure 3.



Figure 3. Stainless steel fiber particulate filter setup to verify the filtration performance.

2.2. Experimental Results of the Stainless Steel Fiber Filter

Variations in the diesel engine exhaust temperature at the different speeds and loads are shown in Figure 4. The figure reveals the following:

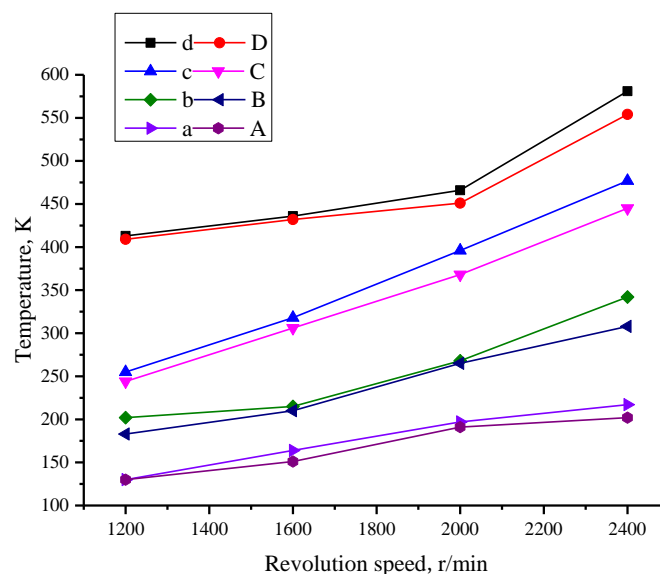


Figure 4. Exhaust temperature change at the different speeds and loads.

(1) The exhaust gas temperatures before and after the stainless steel fiber particulate filter installed under a low load do not greatly differ, however a change is observed before and after the installation of the stainless steel fiber particulate filter under a 75% load at a high speed;

(2) When the speed remains constant, the exhaust temperature changes with the load. However, the temperature change is not obvious with the low-load range. The fuel consumption increases at high speeds and heavy loads, and the exhaust temperature is

high. Incompletely burned fuel continues to burn in the exhaust pipe, resulting in a further increase in the exhaust temperature.

Figure 5 shows the changes in the diesel engine fuel consumption rate at the different speeds and loads. The fuel consumption rate of the diesel engine under a high load changes substantially after the installation of the stainless steel fiber particulate filter. After filter installation, the exhaust pressure increases, resulting in a decrease in the engine performance. The highest fuel consumption rates are found under 25% and 100% loads and should be avoided during actual operation. The diesel engine attains the lowest fuel consumption rate under a 75% load, which indicates an economically feasible consumption rate. The fuel consumption rate after filter installation is approximately 10% higher. Under low-load conditions, although the fuel consumption is relatively high, the generated PM amount is small, and the exhaust flow rate is low. Hence, the exhaust resistance does not change much. Therefore, the fuel consumption rate does not change notably after installation of the stainless steel fiber particulate filter.

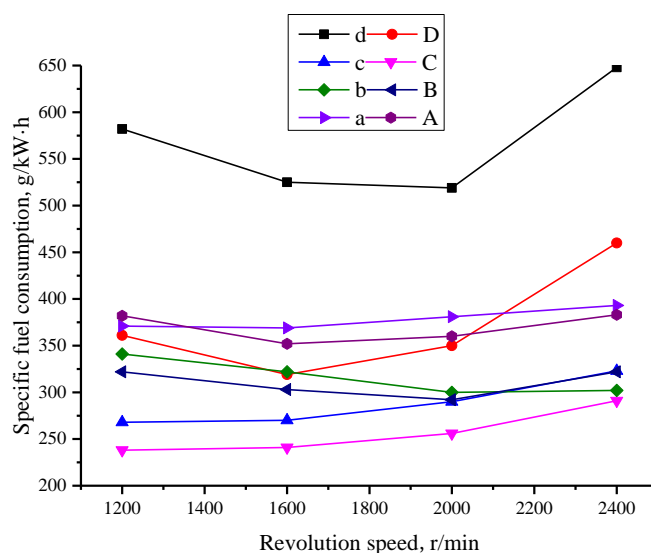


Figure 5. Fuel consumption rate change in the exhaust gas at different speeds and loads.

Figure 6 shows the change in HC content at different speeds and loads. When the filter is installed, the HC content in the exhaust gas increases. This occurs as filter installation increases both the back pressure and fuel consumption rate, which in turn leads to an increase in the HC content in the exhaust gas.

The figure shows that under loads of 25%, 50%, and 75%, the HC content decreases with increasing speed, the HC content increases with increasing load, and the HC content is very high under full-load conditions. After filter installation, under the 100% load, the HC content exhibits a large difference except at 1600 r/min. This occurs as the fuel consumption rate significantly increases after filter installation, however the power does not change, and more fuel is thus incompletely burned. These incomplete combustion products crack in the high-temperature exhaust pipe and produce more HC compounds. In the same manner, the HC content difference at 2400 r/min under the 50% load can be explained.

Figure 7 shows the change in CO content in exhaust gas with speed and load.

Under medium and low loads, the CO content is extremely low. With increasing speed or load, the CO content also increases. Under the 100% load conditions, the CO content considerably changes after filter installation. This occurs as the fuel consumption rate notably increases after installation, and more incomplete combustion products react with oxides (NO_x , O_2 , etc.) in the high-temperature exhaust pipe, which produces more CO. The CO content decreases at 1600 r/min, which is related to the low fuel consumption under this load. Hence, the CO content in the emissions is also reduced. Compared to the other low-load conditions, the 75% load yields a considerable increase in the CO content.

The CO content under the 75% load and lower does not differ much after filter installation. This occurs as under the 75% operating conditions, less PM is generated, imposing little effect on the back pressure of the diesel engine, thus ensuring that the engine operating parameters do not greatly vary.

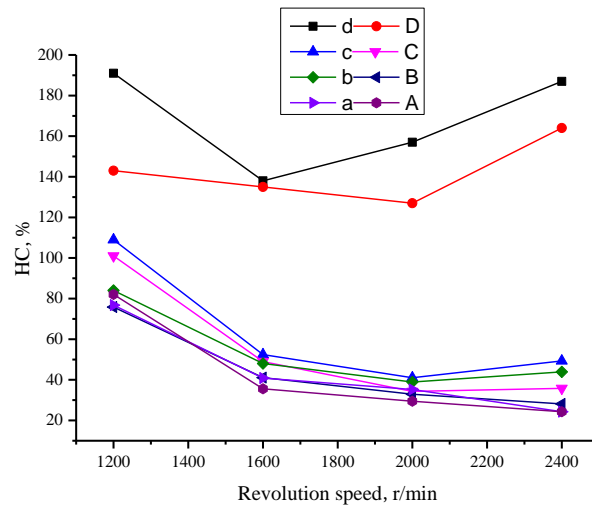


Figure 6. HC content change in the exhaust gas at different speeds and loads.

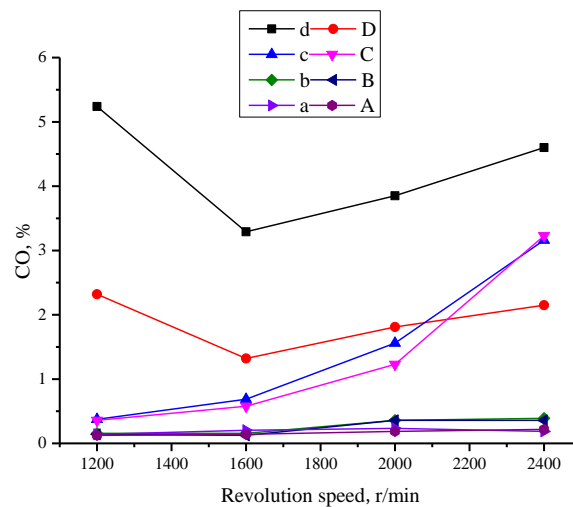


Figure 7. CO content change in the exhaust gas at different speeds and loads.

Figure 8 shows the change in the NO_x content at different speeds and loads. At a speed of 1200 r/min, the load increases from 25% to 50%, and the generated NO_x amount increases. When the load reaches a certain value, the generated NO_x amount begins to decrease. Based on the obtained data, the NO_x content decreases from the 75% to the 100% load conditions. Under full-load conditions, the minimum NO_x content is reached.

The operating conditions for NO_x are high temperature and high pressure with a sufficient reaction time. At low speeds, the NO_x reaction time is relatively sufficient, and the generated NO_x amount is thus relatively large. With increasing speed, the temperature also increases, and the temperature better facilitates NO_x generation than the reaction time does. Under a high load, the exhaust gas temperature is high, however the PM content is also high, which contributes to NO_x reduction. From the perspective of the 75% load, the NO_x content increases considerably with increasing speed, which coincides with the emission temperature comparison chart, indicating that the temperature exhibits a close relationship with NO_x and achieves a positive correlation. Overall, the impact of speed

on NO_x emissions is smaller than that of the load. NO_x generation after filter installation under the various working conditions increases, however the increase is not obvious.

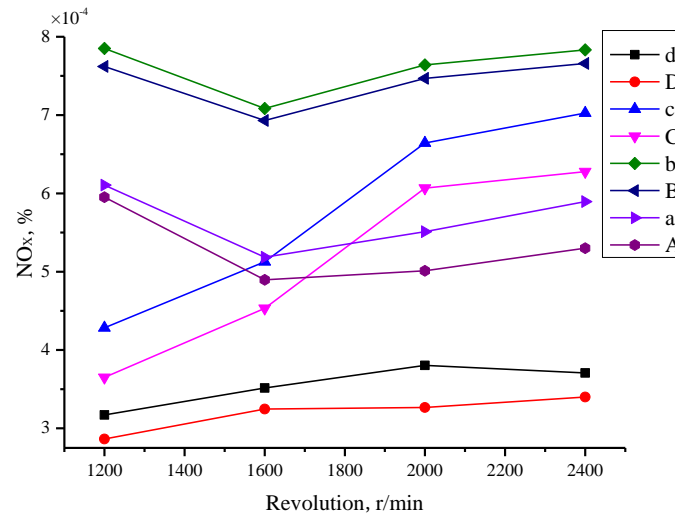


Figure 8. NO_x content change in the exhaust gas at different speeds and loads.

Figure 9 shows the change in the CO₂ content at the different speeds and loads. The CO₂ generation amount slightly decreases with increasing speed under the load conditions of 25%, 50%, and 75%, and the overall change remains relatively consistent. Under loads of 25%, 50%, and 75%, the CO₂ content does not change notably after filter installation, and the CO₂ content change after installation under the 100% load does not differ much. This occurs as the CO₂ volume fraction has nearly reached its limit value under all operating conditions (the highest CO₂ volume fraction measured in the engine test is 17.6%), so the value does not change much.

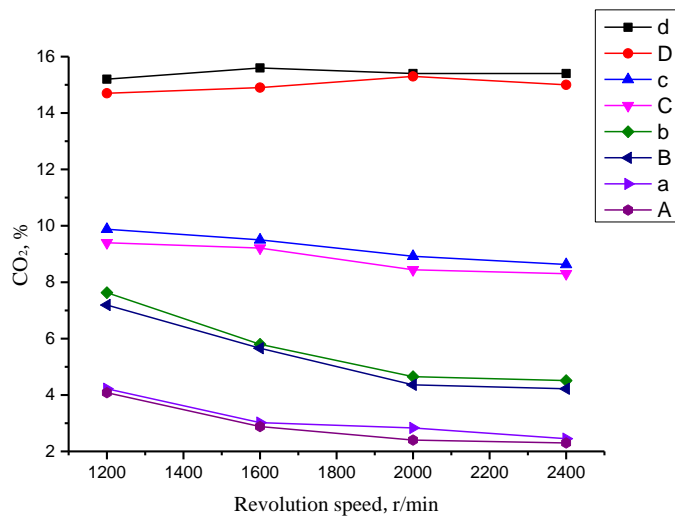


Figure 9. CO₂ content change in the exhaust gas at different speeds and loads.

The exhaust smoke content is expressed by the extinction coefficient *k* of the exhaust. Figure 10 shows a comparison of the exhaust smoke content before and after filter installation under eight working conditions (running 10 min). Overall, the extinction coefficient *k* without filter installation exhibits an exponential increase with increasing speed, which is basically consistent with the fuel consumption trend. After installation, the extinction coefficient *k* can be reduced to a certain extent. The extinction coefficient *k* does not fluctuate much under the 25% and 50% loads, yet still exhibits exponential growth, as shown in

Figure 10. High load means the exhaust gas flow in the filter remains at a high level. The increase in the flow velocity will produce more turbulence in the porous filter element (steel fiber) to a certain extent, so that more particles colliding with the fibers will be captured.

At a rotation speed of 1200 r/min, the extinction coefficient k value is very small. This is attributed to the low rotation speed, long residence time of the emitted PM in the combustion chamber, and sufficient supplementary combustion. Consequently, less PM is emitted. With increasing speed, the emitted PM concentration increases, and the k value correspondingly increases.

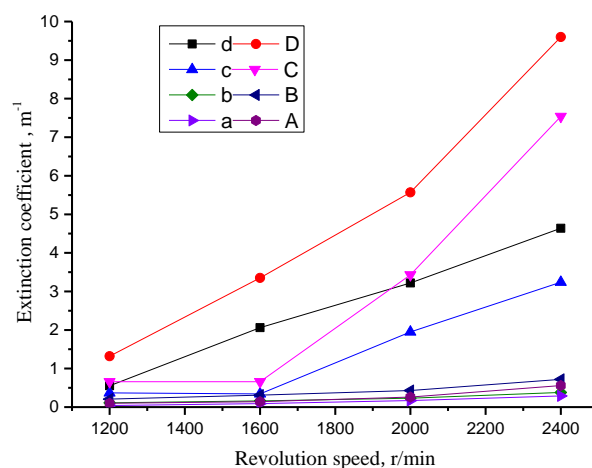


Figure 10. Exhaust smoke comparison.

2.3. Design of the Optimized Muffler

The optimized muffler is a structural improvement of the existing muffler products for R180 diesel engines. It integrates muffling and filtering functionalities. The filter element is easy to disassemble, which is more consistent with the needs of small horsepower non-road diesel engines.

The structure of the original muffler is shown in Figure 11. The upper housing 1 of the original muffler is welded to a transverse perforated pipe 7, and the orifice of the transverse perforated pipe 7 coincides with the exhaust port 6 in the upper housing. The support plate is welded to a longitudinal silencing pipe 8, and all other parts are welded to one another. The entire structure is non-detachable and belongs to a reactive muffler. When the muffler is working, the gas enters the longitudinal perforated pipe from the engine exhaust pipe. At this time, the gas is shunted, and part of the gas continues to flow forward along the original direction and enters the transverse perforated pipe through the small hole on the support plate and the transverse perforated pipe; part of the gas flows to the expansion chamber (composed of longitudinal perforated pipe and lower housing) through the small hole on the perforated pipe. The gas in the expansion chamber passes through the small hole on the support plate, enters the transverse perforated pipe and is discharged together with the previous air flow.

The optimized muffler is shown in Figure 12 and, functions as a resistance composite muffler. The diameter of the inlet and exhaust pipe is 30 mm, the length of the perforated pipe is 100 mm, the diameter of the perforated hole is 4 mm, the inner diameter of the upper and lower shells is 92 mm, and the outer diameter of the filter element is 83 mm. Considering the material selection of the support plate, 1 mm steel plate is used for spinning press, as shown in Figure 13. The stainless steel fibers employed as the filter medium are also good sound-absorbing materials (Figure 13), which plays a role in resistive noise elimination. The pores ensure a certain collection efficiency, and simultaneously, the pores are connected to ensure gas circulation smoothness. When exhaust gas passes through the device, PM is retained in the filter medium. The gas enters longitudinal perforated pipe 14 from exhaust pipe 9 and enters filter element 7 through the small holes in the longitudinal

perforated pipe, then the airflow direction changes. At this time, the filter element (stainless steel fibers) can filter a large proportion of the emitted PM.

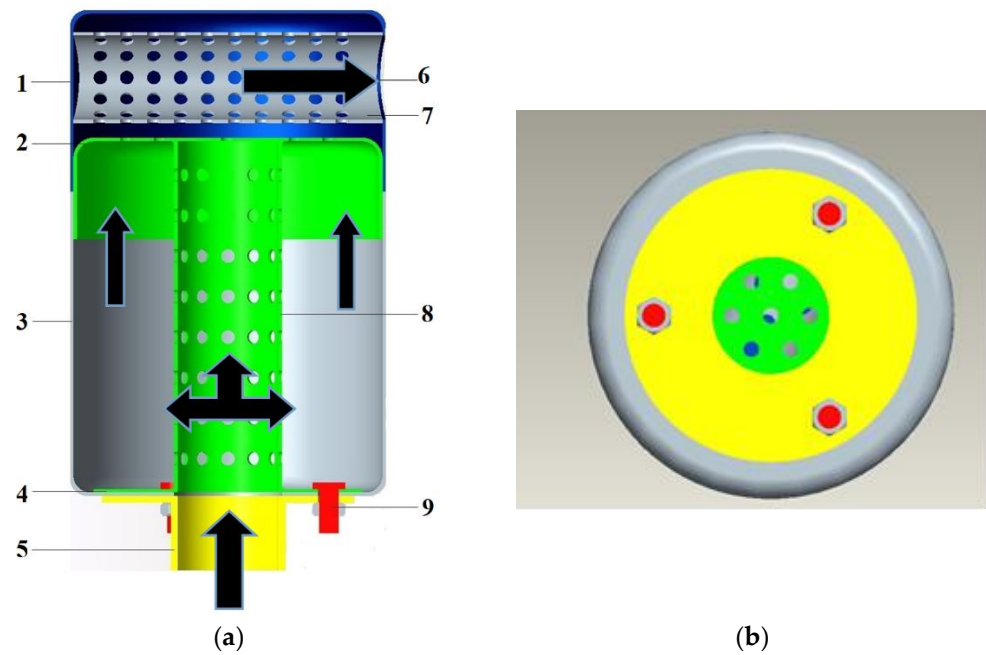


Figure 11. (a) Structure of the original muffler, (b) Upper housing: 1. upper housing; 2. support plate; 3. lower housing; 4. gasket; 5. exhaust pipe; 6. exhaust port; 7. transverse perforated pipe; 8. longitudinal perforated pipe; 9. fixed bolt.

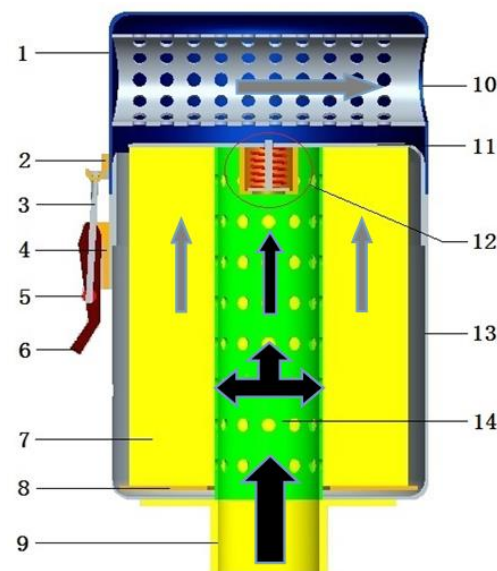


Figure 12. Structure of the optimized muffler: 1. upper housing; 2. locking tongue; 3. adjusting screw; 4. support; 5. adjusting nut; 6. adjusting arm; 7. filter element; 8. gasket; 9. exhaust pipe; 10. exhaust port; 11. support plate; 12. pressure reducing valve; 13. lower housing; 14. longitudinal perforated pipe.



Figure 13. Inside view of the optimized muffler; the muffler filled with stainless steel fibers.

When the optimized muffler is operated for a certain period of time, the PM accumulated in the filter element can seriously hinder the discharge of gas, which can cause a pressure difference between the exhaust pipe and the upper side of support plate 11 (Figure 14). At this time, the pressure difference can overcome the resistance of spring 5, force one-way valve element 4 to open, and make gas flow out of pressure relief hole 3. Untreated exhaust exhibits a strong odor and contains smoke, and a preliminary assessment can be made on whether the filter element should be replaced.

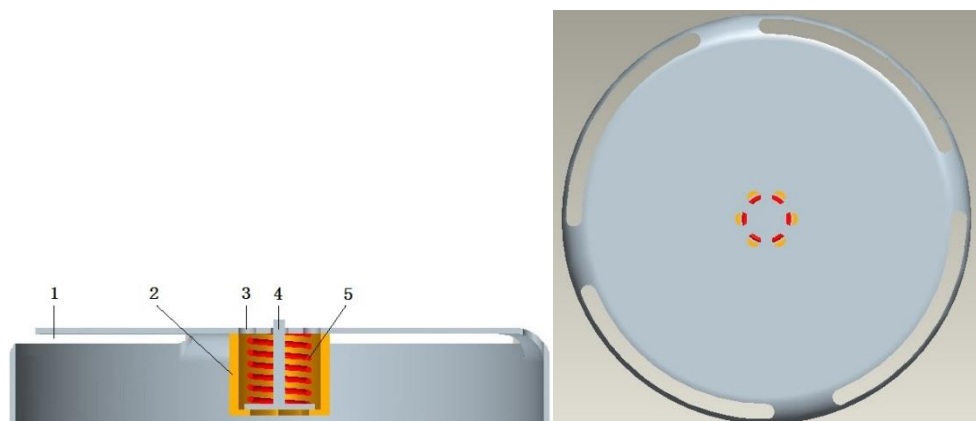


Figure 14. Optimized design of the upper housing. 1. Exhaust hole; 2. pressure valve pipe; 3. pressure relief hole; 4. valve element; 5. spring.

2.4. Simulation

2.4.1. Evaluation Index of Acoustic Performance

There are two main types of indicators of the optimized muffler performance evaluation: acoustic and dynamic performance indicators. The acoustic performance evaluation index mainly includes insertion and transmission losses, and the aerodynamic index mainly includes the pressure loss and power loss ratio.

The transmission loss L_{TL} refers to the difference in sound power at the inlet and outlet of the muffler, and the calculation equation is:

$$L_{TL} = L_{W_1} - L_{W_2} = 10 \lg \frac{W_1}{W_2} \quad (1)$$

In Equation (1), the sound power level at the inlet of the muffler denoted as L_{W_1} , the sound power level at the outlet denoted as L_{W_2} (in dB), the sound power at the inlet denoted as W_1 , and the sound power at the outlet denoted as W_2 (in W).

The transmission loss reflects only the acoustic characteristics of the muffler itself, which is only directly related to the structural form and unaffected by external factors.

Insertion loss L_{IT} is the difference in sound power level or sound pressure level at the exit position of the optimized muffler before and after installation and is expressed as follows:

$$L_{IT} = L_{W_i} - L_{W_t} = 10 \lg \frac{W_i}{W_t} \quad (2)$$

In Equation (2), the sound power level of a certain measuring point before the installation of the muffler is L_{W_i} , the sound power level after installation is L_{W_t} , and the unit is dB; the sound power of a certain measuring point before installation is W_i , the sound power after installation is W_t , and its unit is W.

There is a relatively simple method to measure the insertion loss, which does not have very high requirements for the measurement environment, so it is easy to implement. The measurement result can reflect the noise reduction performance of the muffler itself, and the external comprehensive acoustic performance.

The pressure loss ΔP is the average total pressure difference between the inlet and the outlet when a certain amount of smooth air flow passes through. As the optimized muffler in this study has equal cross-sectional area at both ends, the static air pressure difference can be considered as the pressure loss.

$$\Delta P = P_1 - P_2 \quad (3)$$

In Equation (3), P_1 is the exhaust pressure at the inlet; P_2 is the exhaust pressure at the outlet.

The power loss ratio R_N is the percentage of the difference in power before and after the optimized muffler is installed when the engine is under the calibrated operating conditions, i.e.,

$$R_N = \frac{P_{e1} - P_{e2}}{P_{e1}} \times 100\% \quad (4)$$

In Equation (4), P_{e1} and P_{e2} are the engine power before and after the optimized muffler is installed, respectively, and the unit is kW.

The power loss ratio reflects the impact of resistance loss on the engine performance. When measuring the power loss ratio, the engine state and test environment should not change, and generally control $R_N \leq 5\%$.

Based on the requirements of the problem, this paper uses the transmission loss L_{TL} and pressure loss ΔP as the acoustic performance and aerodynamic evaluation indicators of the simulation analysis, respectively.

2.4.2. Simulation Model

Assuming that the gas flow in the optimized muffler is axisymmetric, a two-dimensional mesh model is generated by choosing half of the model. The model in this paper does not consider the effects of heat and mass transfer in the optimized muffler and assumes that the gas velocity distribution is uniform when gas enters the optimized muffler. Then, a two-dimensional axisymmetric steady-state incompressible flow model is established. The governing equations of the flow and the turbulence model have been verified in previous research [41–44].

3. Performance of the Optimized Muffler

3.1. Analysis of the Acoustic Performance

The working environment of the diesel engine is a confined space. In addition, during operation of the diesel engine, it is necessary to activate the laboratory ventilation device to assist with exhaust gas. Furthermore, it is necessary to activate the water pump to supply water to the dynamometer. Therefore, there are many noise sources in the laboratory environment, and the exhaust noise measured in the test is extremely complex. To better

reflect the silencing amount of the proposed device, the FLUENT acoustic module is employed to conduct acoustic simulations of the optimized muffler.

Two-dimensional modeling of the optimized muffler is performed in Gambit 2.4.6, as shown in Figure 15. Then, the turbulence model parameters are set in FLUENT 14.

The exhaust flow rate at the inlet is 140.2 m/s (1200 r/min), the temperature is 500 K, the porosity of the porous media is set to 90%, the porous viscous resistance coefficient C_1 is 3.84×10^9 , the internal resistance coefficient C_2 is 20,414, the static pressure is 151.99 kPa, and the exhaust dynamic viscosity is 1.824×10^{-5} . The Reynolds number Re is 9.21×10^4 , and the internal flow is thus turbulent. Hence, the standard $k-\epsilon$ model is adopted. The turbulence intensity at the inlet and outlet is 10%. All walls are set as non-slip boundaries, and the standard wall equation is adopted.

The following simulation results are obtained: before adding the stainless steel fibers, the noise in the optimized muffler is high, especially low-frequency noise, mainly below 5 kHz, and the total sound pressure level reaches approximately 100 dB (as shown in Figure 16). After the installation of stainless steel fiber in the optimized muffler, low-frequency noise is significantly reduced, and the sound power is evenly distributed at each frequency. The total sound pressure level reaches approximately 85 dB (as shown in Figure 16). Through simulation analysis and comparison, the noise level decreases by approximately 15% after stainless steel fibers have been added to the optimized muffler.

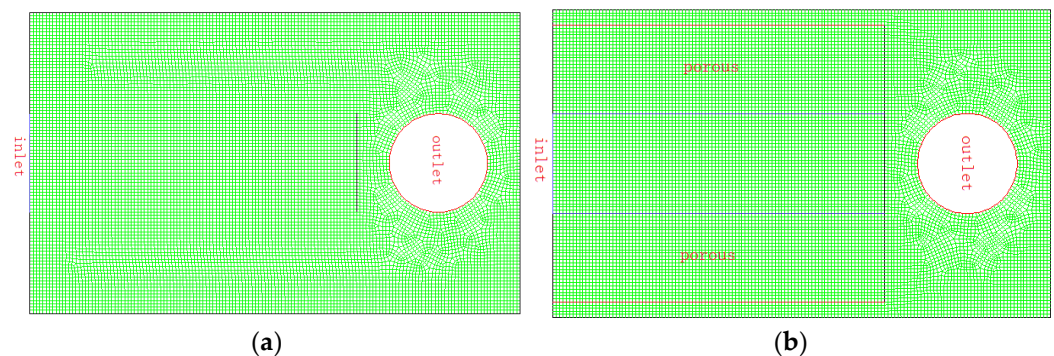


Figure 15. Two dimensional model of the optimized muffler. (a) without stainless steel fibers, (b) with stainless steel fibers.

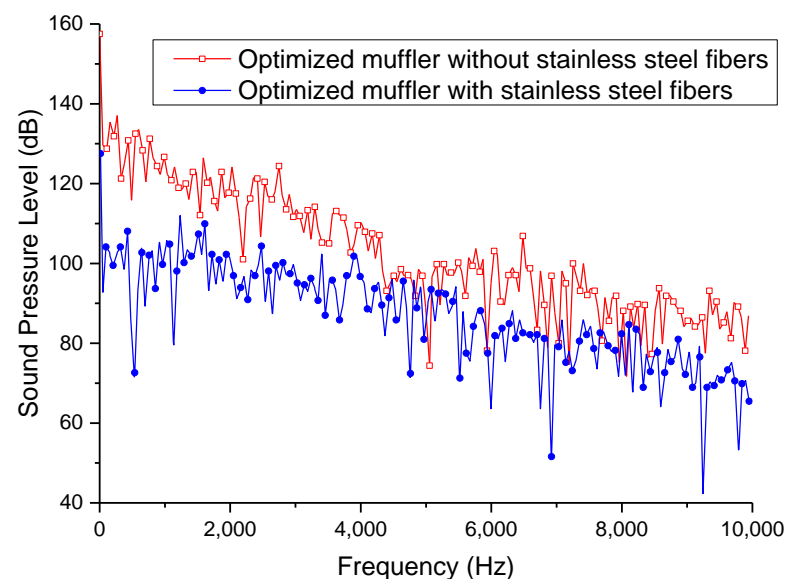


Figure 16. Sound pressure simulation of the optimized muffler with and without stainless steel fibers.

3.2. Experimental Validation of the Extinction Coefficient

The optimized muffler was directly connected to the exhaust pipe where the steel fiber PM filter was (Figure 2), and the smoke level was compared under eight working conditions (running 10 min) as shown in Figure 17. Overall, except for the 25% load, the extinction coefficient k of the device without stainless steel fibers increases exponentially with increasing speed, and this trend becomes increasingly obvious with increasing load. After adding stainless steel fibers, the extinction coefficient k can be greatly reduced, reaching 60%. The higher the load is, the more obvious the reduction in the extinction coefficient k , which verifies the effect of the optimized muffler on the PM removal from the exhaust.

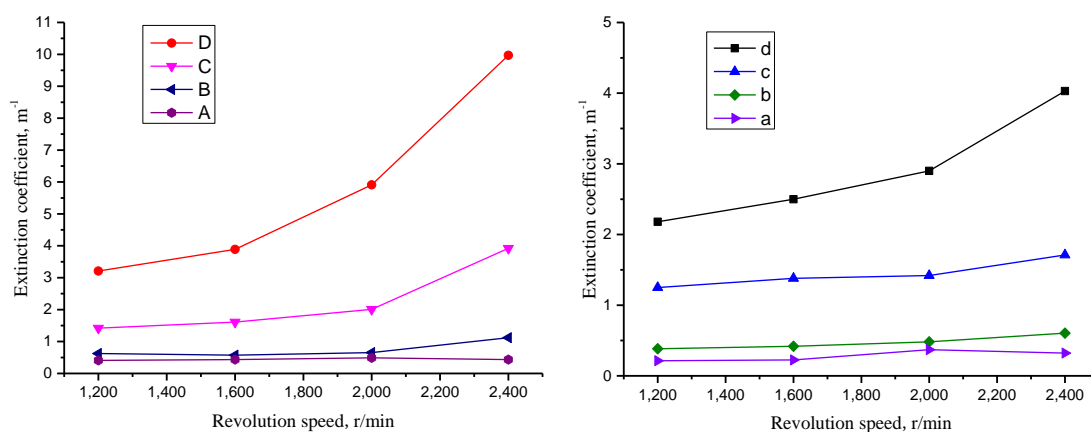


Figure 17. Extinction coefficient comparison of the optimized muffler with and without stainless steel fiber.

4. Conclusions

A test bench for the R180 diesel engine commonly applied in agriculture was built, and stainless steel fibers were employed as a filter medium to trap emitted diesel-related PM. The engine working conditions included various speeds (1200, 1600, 2000 and 2400 r/min) and loads (25%, 50%, 75%, and 100%), the HC, CO, NO_x, and CO₂ volume fractions in the exhaust were measured during the test, and the exhaust temperature, fuel consumption rate and extinction coefficient were also determined. A comparison of the test results with and without stainless steel fibers was conducted. Through comparison, it was found that the installation of steel fibers could increase the exhaust temperature and fuel consumption under the same working conditions. The installation of steel fibers could increase the HC, CO, NO_x, and CO₂ volume fractions to different degrees, however the increase remained limited. However, steel fibers could reduce the extinction coefficient to a large extent, which verified the notable function of steel fibers in PM capture.

An improved muffler integrated with the functions of PM filtration and noise reduction was designed, by using the steel fibers as the filtration medium. The simulation results for the optimized muffler verified the filtering and muffling performance. The optimized muffler performance is as follows: under a full load, the extinction coefficient K could be reduced by approximately 60%, and the noise level could be reduced by approximately 15%.

The whole optimized muffler is a mechanical structure with good reliability, and the use and maintenance costs are very low, which can satisfy the requirements of agricultural machinery with a low power level.

Author Contributions: Conceptualization, M.M. and L.F.; methodology, M.M.; validation, X.M.; formal analysis, M.M.; investigation, M.M., X.M., X.H. and L.D.; resources, M.M., X.M. and X.H.; writing—original draft preparation, C.S. and L.F.; writing—review and editing, L.D., B.C. and X.W.; supervision, M.M., B.C. and L.F.; project administration, B.C.; funding acquisition, M.M. All authors have read and agreed to the published version of the manuscript.

Funding: This research was funded by Shandong Provincial Natural Science Foundation, China, (Grant No. ZR2020QE164, ZR2021QA071), and Foundation of State Key Laboratory of High-efficiency Utilization of Coal and Green Chemical Engineering (Grant No. 2022-K64).

Institutional Review Board Statement: Not applicable.

Informed Consent Statement: Not applicable.

Data Availability Statement: Not applicable.

Acknowledgments: The authors are very thankful to the editor and referees for their valuable comments and suggestions for improving the paper.

Conflicts of Interest: The authors declare no conflict of interest.

References

1. Yu, B.; Zhao, G.; An, R. Framing the picture of energy consumption in China. *Nat. Hazards* **2019**, *99*, 1469–1490. [[CrossRef](#)]
2. Wang, S.; Sun, S.; Zhao, E.; Wang, S. Urban and rural differences with regional assessment of household energy consumption in China. *Energy* **2021**, *232*, 121091. [[CrossRef](#)]
3. Zheng, S.; Wang, J.; Sun, C.; Zhang, X.; Kahn, M.E. Air pollution lowers Chinese urbanites' expressed happiness on social media. *Nat. Hum. Behav.* **2019**, *3*, 237–243. [[CrossRef](#)]
4. Lowe, S.R.; Wang, C.; Ma, Y.; Chen, K. Particulate matter pollution and risk of outpatient visits for psychological diseases in Nanjing, China. *Environ. Res.* **2021**, *193*, 110601. [[CrossRef](#)] [[PubMed](#)]
5. Wu, J.; Tian, Y.; Wu, Y.; Wang, Z.; Wu, Y.; Wu, T.; Qin, X.; Wang, M.; Wang, X.; Wang, J.; et al. Seasonal association between ambient fine particulate matter and venous thromboembolism in Beijing, China: A time-series study. *Environ. Sci. Pollut. Res.* **2021**, *28*, 32795–32801. [[CrossRef](#)] [[PubMed](#)]
6. Wang, P. China's air pollution policies: Progress and challenges. *Curr. Opin. Environ. Sci. Health* **2021**, *19*, 100227. [[CrossRef](#)]
7. Ministry of Ecology and Environment. *Technical Guidelines for Compilation of Non-Road Mobile Source Emission Inventories*; Ministry of Ecology and Environment: Beijing, China, 2015.
8. Ministry-of-Ecology-and-Environment. *China Mobile Source Environmental Management Annual Report (2021)*; Ministry and Ecology and Environment: Beijing, China, 2021.
9. Lang, J.; Tian, J.; Zhou, Y.; Li, K.; Chen, D.; Huang, Q.; Xing, X.; Zhang, Y.; Cheng, S. A high temporal-spatial resolution air pollutant emission inventory for agricultural machinery in China. *J. Clean. Prod.* **2018**, *183*, 1110–1121. [[CrossRef](#)]
10. Desouza, C.D.; Marsh, D.J.; Beevers, S.D.; Molden, N.; Green, D.C. Real-world emissions from non-road mobile machinery in London. *Atmos. Environ.* **2020**, *223*, 117301. [[CrossRef](#)]
11. Guo, X.; Wu, H.; Chen, D.; Ye, Z.; Shen, Y.; Liu, J.; Cheng, S. Estimation and prediction of pollutant emissions from agricultural and construction diesel machinery in the Beijing-Tianjin-Hebei (BTH) region, China. *Environ. Pollut.* **2020**, *260*, 113973. [[CrossRef](#)]
12. Zhang, Q.; Wei, N.; Yang, L.; Feng, X.; Zhang, Y.; Wu, L.; Mao, H. Emission inventory and control policy for non-road construction machinery in Tianjin. *Environ. Sci. Pollut. Res.* **2022**, *29*, 6688–6697. [[CrossRef](#)]
13. Hou, X.; Tian, J.; Song, C.; Wang, J.; Zhao, J.; Zhang, X. Emission inventory research of typical agricultural machinery in Beijing, China. *Atmos. Environ.* **2019**, *216*, 116903. [[CrossRef](#)]
14. Ye, Z.; Li, Z.; Huang, J.; Gong, M. Study on Air Pollutant Emission Inventory of Typical Non-road Mobile Machineries in Guangzhou. *Environ. Sci. Manag.* **2018**, *43*, 63–66. [[CrossRef](#)]
15. Bian, Y.; Fan, X.; Li, C.; Ye, X.; Wang, X.; Huang, Z.; Zheng, J. A sector-based emission inventory and its uncertainty from non-road mobile machinery in Guangdong Province, China. *Acta Sci. Circumstantiae* **2018**, *38*, 2167–2178. [[CrossRef](#)]
16. Wang, F.; Li, Z.; Zhang, K.; Di, B.; Hu, B. An overview of non-road equipment emissions in China. *Atmos. Environ.* **2016**, *132*, 283–289. [[CrossRef](#)]
17. Li, C. *Emissions Characteristics and Future Trends of Non-Road Mobile Sources in China*; South China University of Technology: Guangzhou, China, 2017.
18. Ma, S. Non-road Mobile Source Emission Inventory of Chengdu from 2011 to 2015. *Sichuan Environ.* **2018**, *37*, 33–37. [[CrossRef](#)]
19. Gao, C.; You, H.; Ba, Q.; Liang, C. Study on a Non-road Mobile Source Emission Inventory and Scenario Prediction in Northeast China. *J. Northeast. Univ. (Nat. Sci.)* **2021**, *42*, 358–366. [[CrossRef](#)]
20. Pang, S.; Yang, X. The Current Situation and Pollution Prevention and Control Exploration of Non-road Motor Vehicles in Mianyang City. *Sichuan Environ.* **2018**, *37*, 169–172.
21. Ann Arbor, M.; Arlington, V. *User's Guide for the Final NONROAD2005 Model*; Environmental Protection Agency: Washington, DC, USA, 2005.
22. CARB. *User's Guide for OFFROAD2007*; California Air Resources Board: Sacramento, CA, USA, 2007.
23. European Environment Agency. *EMEP/CORINAIR Emission Inventory Guidebook-2007*; Guidebook, Emission Inventory; European Environment Agency: Copenhagen, Denmark, 2007.
24. Lewis, P.; Rasdorf, W.; Frey, H.C.; Pang, S.-H.; Kim, K. Requirements and Incentives for Reducing Construction Vehicle Emissions and Comparison of Nonroad Diesel Engine Emissions Data Sources. *J. Constr. Eng. Manag.* **2009**, *135*, 341–351. [[CrossRef](#)]

25. Hoult, J.; Weeda, D. The EPA Non-road Diesel Tier 4 Final Rule. *Eng. Technol. A Sustain. World* **2010**, *17*, 10–12.
26. EPA. *Final Rule for Control of Emissions of Air Pollution From Nonroad Diesel Engines and Fuel*; Environmental Protection Agency: Washington, DC, USA, 2004.
27. Kuklinska, K.; Wolska, L.; Namiesnik, J. Air quality policy in the U.S. and the EU—A review. *Atmos. Pollut. Res.* **2015**, *6*, 129–137. [[CrossRef](#)]
28. Waluś, K.J.; Warguła, L.; Krawiec, P.; Adamiec, J.M. Legal regulations of restrictions of air pollution made by non-road mobile machinery—the case study for Europe: A review. *Environ. Sci. Pollut. Res.* **2018**, *25*, 3243–3259. [[CrossRef](#)] [[PubMed](#)]
29. Kanagawa, H.; Nakayama, Y.; Sakai, N.; Soma, Y.; Kane, S. *Environmental Law and Practice in Japan: Overview*; Kanagawa International Law Office: Tokyo, Japan, 2021.
30. GB20891-2007; Limits and Measurement Methods for Exhaust Pollutants from Diesel Engines of Non-Road Mobile Machinery (I, II). SEPA: Beijing, China, 2007.
31. GB20891-2014; Limits and Measurement Methods for Exhaust Pollutants from Diesel Engines of Non-Road Mobile Machinery (CHINA III, IV). SEPA: Beijing, China, 2014.
32. HJ1014-2020; Emissions Control Technical Requirements of Non-Road Diesel Mobile Machinery. Ministry-of-Ecology-and-Environment: Beijing, China, 2020.
33. GB36886-2018; Limits and Measurement Methods for Exhaust Smoke from Non-Road Mobile Machinery Equipped with Diesel Engine. Ministry-of-Ecology-and-Environment: Beijing, China, 2018.
34. Liu, Y. Present Situation and Technology of Exhaust Emission Control for Non-Road Mobile Machinery. *Manag. Technol. SME* **2017**, *10*, 115–116. [[CrossRef](#)]
35. Su, Z.; Wang, J.; Zhang, C. After-treatment Technology of the Non-road Machinery Diesel Engine: A Review. *Constr. Mach. Maint.* **2018**, *1*, 41–45. [[CrossRef](#)]
36. Chen, X.; Ju, Y.; Zhang, Q.; Liu, Z.; Wang, Z.; Zhou, D.; Zhao, H.; Chen, G. Key Technologies for Non-road Diesel Engine to Meet National Stage 3 Emissions Regulation. *Mod. Veh. Power* **2015**, *3*, 1–6. [[CrossRef](#)]
37. Presti, M. Optimizing the Exhaust Gas Aftertreatment of Future Agricultural Machinery. *ATZheavy Duty Worldw.* **2019**, *12*, 38–41. [[CrossRef](#)]
38. Zhang, X.; Liang, J. Study on the NRTC Test of Non-road Diesel Engine under China IV Emission Standards. *China Stand.* **2017**, *4*, 18–19. [[CrossRef](#)]
39. Zhang, Q.; Chen, X.; Zhang, K.; Baikang, X.; Li, F. An Experimental Study on NO₂ Emission of Non-Road Diesel Engines. *Mod. Veh. Power* **2015**, *1*, 30–34. [[CrossRef](#)]
40. Guan, J.; Li, M. Off-road Power Technology Research for Meeting U.S. EPA Tier4 Emission Requirements. *Mod. Veh. Power* **2015**, *1*, 16–18. [[CrossRef](#)]
41. Mu, M.; Li, X.; Qiu, Y.; Shi, Y. Study on a New Gasoline Particulate Filter Structure Based on the Nested Cylinder and Diversion Channel Plug. *Energies* **2019**, *12*, 2045. [[CrossRef](#)]
42. Mu, M.; Dou, L.; Aslam, J.; Chen, B. Synergy Analysis of the Influence of the Connection Cone on the Thermal Distribution during Regeneration. *Symmetry* **2021**, *13*, 995. [[CrossRef](#)]
43. Mu, M.; Feng, L.; Zhang, Q.; Zang, W.; Wang, H. Study on abrasive particle impact modeling and cutting mechanism. *Energy Sci. Eng.* **2022**, *10*, 96–119. [[CrossRef](#)]
44. Ding, B.; Feng, W.-C.; Fang, J.; Li, S.-Z.; Gong, L. How natural convection affect cooling performance of PCM heat sink. *Int. J. Heat Mass Transf.* **2022**, *184*, 122272. [[CrossRef](#)]